

Electronic Supplementary Information (ESI) for Chem. Sci.

Quasi-single-crystalline CoO Hexagrams with Abundant Defects for Highly Efficient Electrocatalytic Water Oxidation

Zuozhong Liang,^a Zhehao Huang,^c Haitao Yuan,^a Zhiyuan Yang,^a Chaochao Zhang,^a Yang Xu,^a Wei Zhang,^a Haoquan Zheng,^{*a} and Rui Cao^{*ab}

^a Key Laboratory of Applied Surface and Colloid Chemistry, Ministry of Education, School of Chemistry and Chemical Engineering, Shaanxi Normal University, Xi'an 710119, China.

^bDepartment of Chemistry, Renmin University of China, Beijing, 100872, China.

^cDepartment of Materials and Environmental Chemistry, Stockholm University, SE-10691 Stockholm, Sweden.

Correspondence Email: zhenghaoquan@snnu.edu.cn; ruicao@ruc.edu.cn

Table S1. Comparison of water oxidation performance of Co-based materials.

Catalysts	Electrode	Electrolyte (M, KOH)	Overpotential at 10 mA cm ⁻² (mV)	Reference
P-400	GC	1	269	This work
Co(OH)F	GC	1	313	<i>Adv. Mater.</i> 2017 , 29, 1700286
Ag-CoSe ₂	GC	0.1	320	<i>Angew. Chem. Int. Ed.</i> 2017 , 56, 328
Fe-Co oxide	GC	1	308	<i>Adv. Mater.</i> 2017 , 29, 1606793
Co ₃ O ₄ @CoP	Ni foil	1	238	<i>Adv. Energy Mater.</i> 2017 , 7, 1602643
Co@CoO _x	GC	1	289	<i>Chem. Commun.</i> 2017 , 53, 9277
CoO	GC	1.0	312	<i>Sci. Bull.</i> 2017 , 62, 626
NiCoP/rGO	carbon fiber paper	1	270	<i>Adv. Funct. Mater.</i> 2016 , 26, 6785
Co ₃ O ₄	FTO	1	376	<i>Adv. Energy Mater.</i> 2016 , 6, 1600697
Ni-Co oxide	GC	1	380	<i>Adv. Mater.</i> 2016 , 28, 4601
Co-Bi	GC	1	290	<i>Angew. Chem. Int. Ed.</i> 2016 , 55, 2488
Co@Co ₃ O ₄	GC	0.1	410	<i>Angew. Chem. Int. Ed.</i> 2016 , 55, 4087
NiCo ₂ O ₄	GC	1	290	<i>Angew. Chem. Int. Ed.</i> 2016 , 55, 6290
CoN	Ni foam	1	290	<i>Angew. Chem. Int. Ed.</i> 2016 , 55, 8670
Co ₃ O ₄	GC	0.1	390	<i>Angew. Chem. Int. Ed.</i> 2016 , 55, 9055
MnCoP	GC	1	330	<i>J. Am. Chem. Soc.</i> 2016 , 138, 4006
CoNi(OH) _x	Cu foil	1	280	<i>Adv. Energy Mater.</i> 2016 , 6, 1501661
Co-P film	Cu foil	1	345	<i>Angew. Chem. Int. Ed.</i> 2015 , 54, 6251
Co ₃ O ₄ /NiCo ₂ O ₄	GC	1	340	<i>J. Am. Chem. Soc.</i> 2015 , 137, 5590
Co	GC	0.1	390	<i>J. Am. Chem. Soc.</i> 2015 , 137, 7071

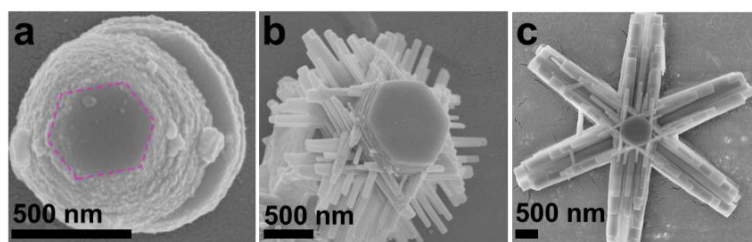


Fig. S1. SEM images of the samples prepared with different reaction times (a) 0.75 h, (b) 1.0 h, and (c) 1.5 h.

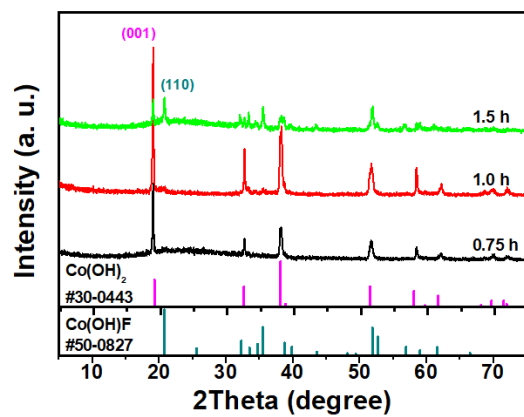


Fig. S2. PXRD patterns of the samples prepared with different reaction times.

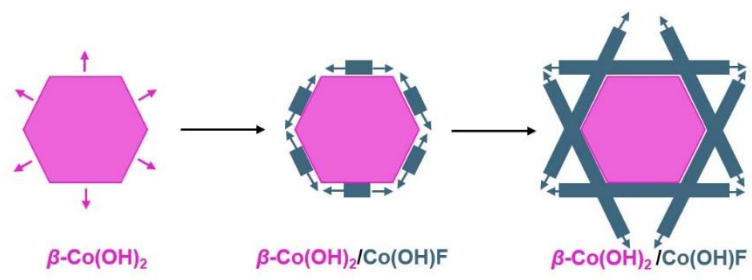


Fig. S3. The scheme of the growth orientation of the $\beta\text{-Co(OH)}_2/\text{Co(OH)F}$ material.

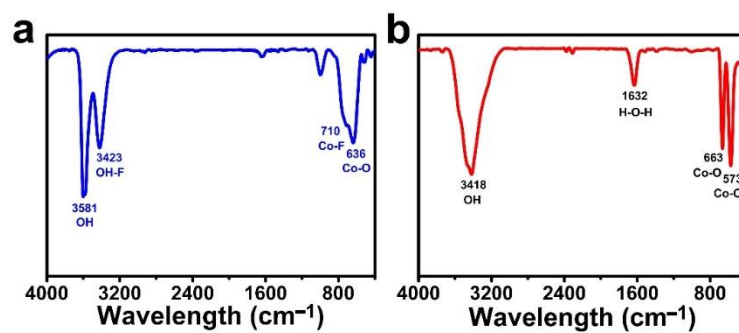


Fig. S4. FTIR spectra of the as-prepared six-branched β -Co(OH)₂/Co(OH)F hexagrams (a) and P-400 (b).

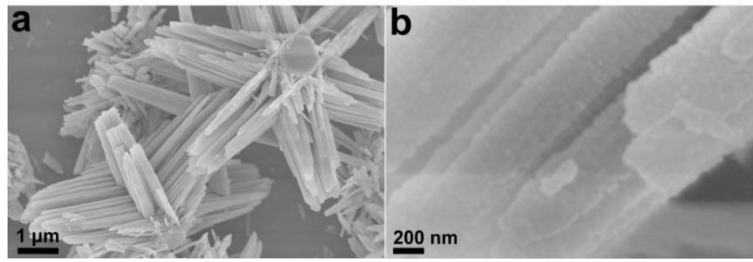


Fig. S5. SEM images of quasi-single-crystalline CoO hexagrams (P-400).

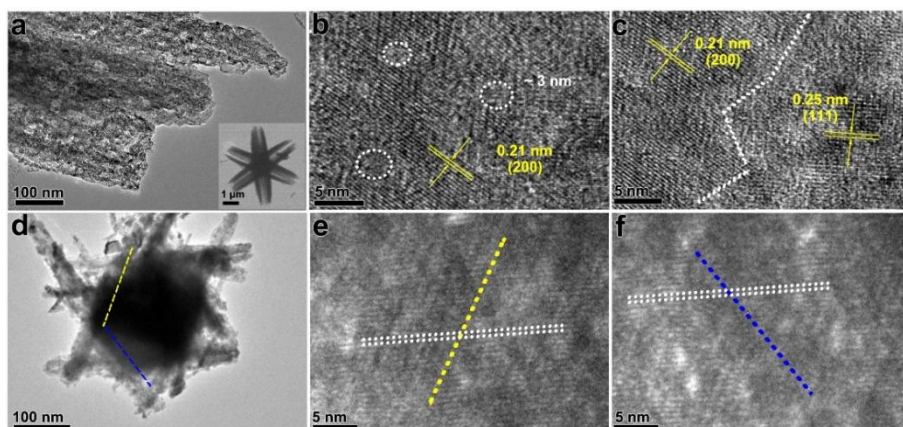


Fig. S6. TEM (a, d) and HRTEM (b, c, e, and f) images of P-400.

As shown in Fig. S6, P-400 remained the hexagram superstructure with roughened surface, indicating the generation of more edge defects during the phase transfer process. TEM image shows porous defects on the branches with a diameter of ~ 3 nm (Fig. S6b). The identified lattice spacings of 0.21 and 0.25 nm can be assigned to the (200) and (111) facets of CoO, respectively (Fig. S6c). Importantly, HRTEM confirmed the relatively regular atomic arrangement in the crystal lattice of P-400, although many atoms were misplaced from their regular positions. These misplacements are indicative of intrinsic defects.

It is a hierarchical structure of the CoO hexagram. Thus, it is important to observe the connection between nanorod branches and the nanoplate core in TEM image. However, the connections is too thick to observe directly by TEM and SAED. We crushed P-400 into small pieces. Fig. S6d shows the TEM image of a piece of crushed P-400 hexagram. The boundaries between nanorods and the nanoplate were obtained from two different edges. The HRTEM images of these boundaries show that the crystal lattices of nanorods and the nanoplate are continuously connected at the atomic level (Fig. S6e, f).

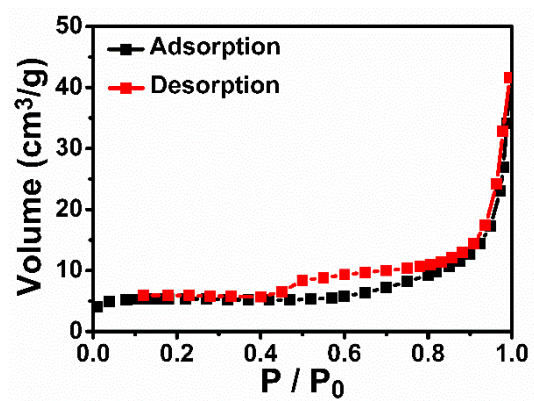


Fig. S7. The N₂ adsorption-desorption curves of the CoO hexagrams (P-400).

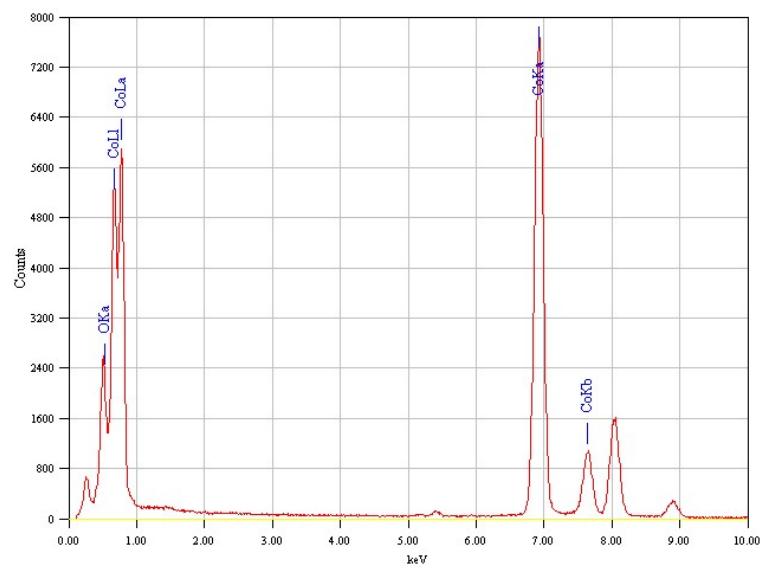


Fig. S8. EDS spectrum of P-400.

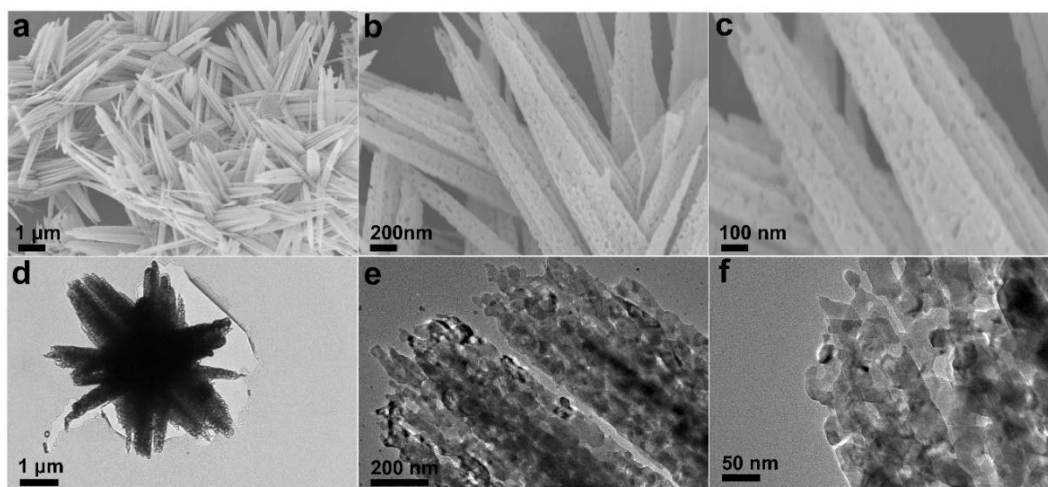


Fig. S9. SEM (a-c) and TEM (d-f) images of P-600.

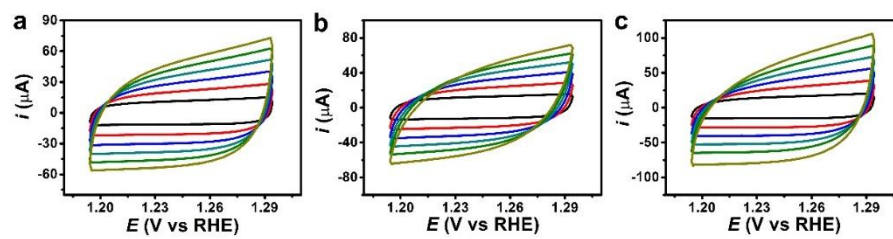


Fig. S10. The charging currents of CoO nanoplates (a), CoO nanorods, (b) and P-400 (c) recorded in the non-Faradaic potential region at different scan rates (10, 20, 30, 40, 50, 60 mV s^{-1}).

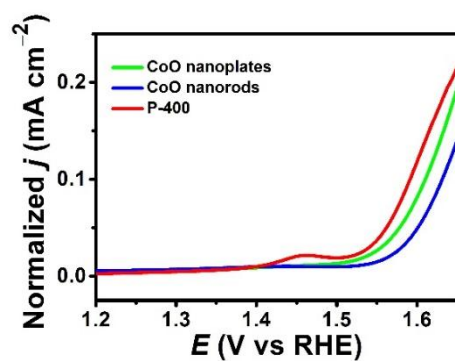


Fig. S11. Normalized current density based on the calculated ECSA of CoO nanoplates, CoO nanorods, and P-400 measured in 1.0 M KOH solution.

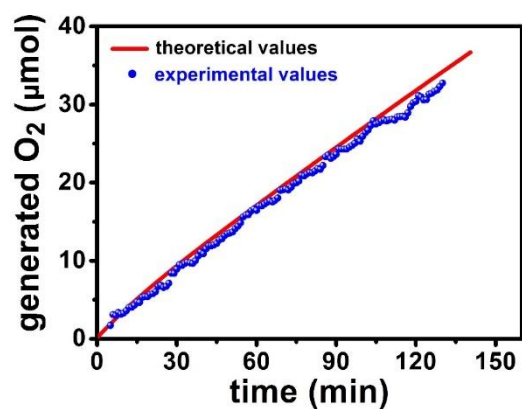


Fig. S12. Experimental (blue dots, from O₂ sensor analysis) and theoretical (red line, from transferred charge) amounts of O₂ generated during controlled potential electrolysis at 1.60 V (vs RHE) with P-400 coated on an ITO electrode. The Faradaic efficiency is calculated to be 98%.

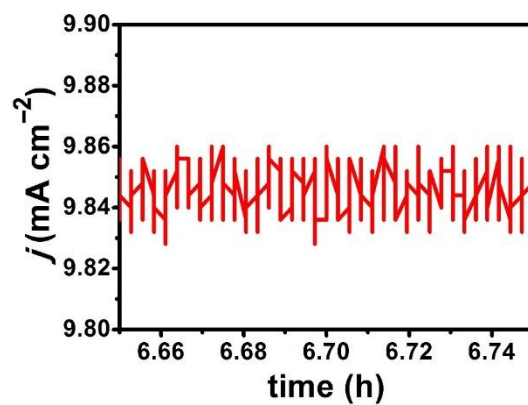


Fig. S13. The expanded current profile during controlled potential electrolysis at 1.60 V (vs RHE) for P-400. The current oscillation indicates the generation and the release of O_2 bubbles on the electrode surface.

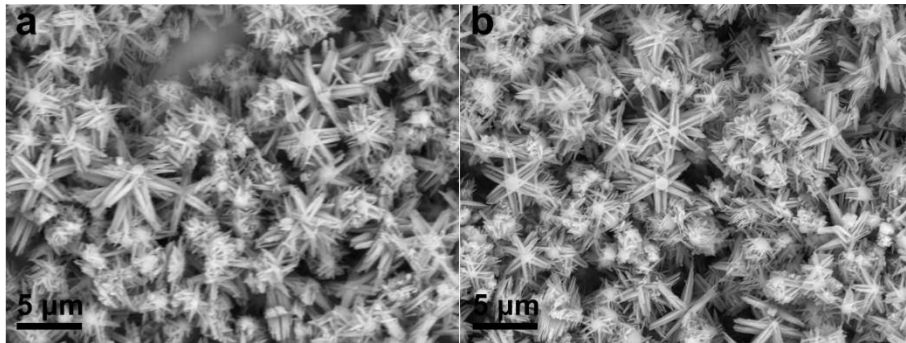


Fig. S14. SEM images of P-400 before (a) and after (b) electrolysis.

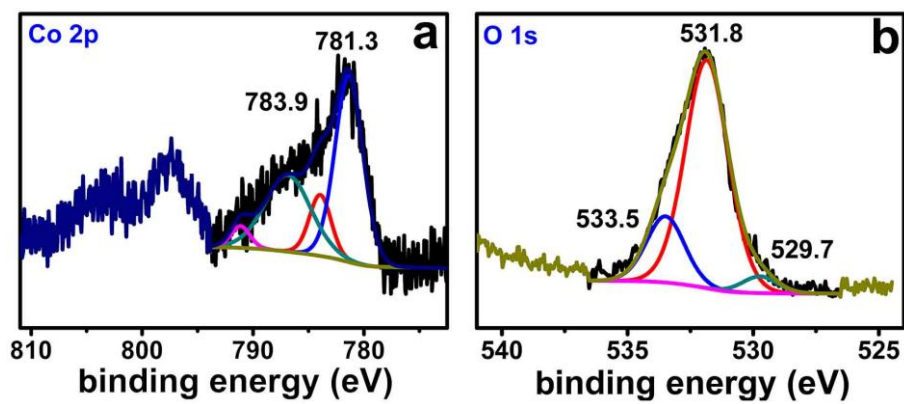


Fig. S15. XPS spectra of P-400 after electrolysis. (a) Co 2p and (b) O 1s energy regions.

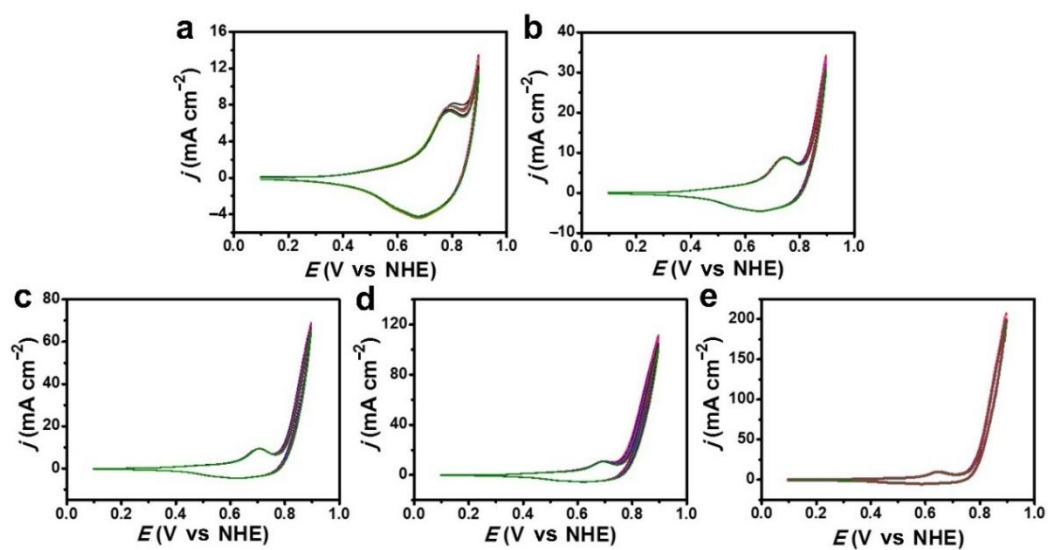


Fig. S16. Consecutive 10-cycle CVs from freshly prepared GC electrodes coated with P-400 in KOH solutions with different concentrations: (a) 0.1 M, (b) 0.2 M, (c) 0.5 M, (d) 1.0 M and (e) 2.0 M. The bubbles on the electrode surface were eliminated after each scan cycle. The iR compensation was conducted before each scan cycle. The last CV scans are extracted to be compared in Figure 5d and 5e.

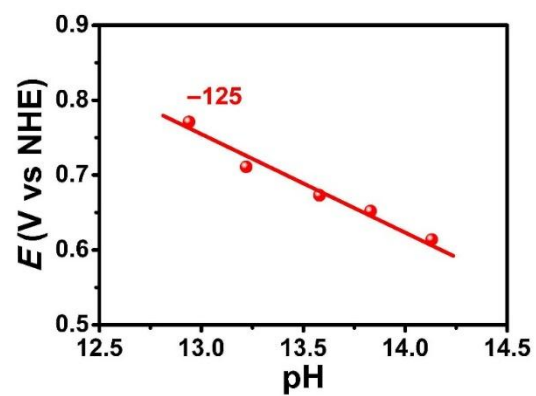


Figure S17. pH dependence of the potential required for P-400 to get a specific current density at $j = 7 \text{ mA cm}^{-2}$.